PERSPECTIVE • **OPEN ACCESS**

Accelerated discovery of multinary chalcogenide quantum dots: combining aqueous chemistry with high-throughput experimentation and machine learning

To cite this article: Oleksandr Stroyuk *et al* 2025 *Nano Futures* **9** 042505

NANO FUTURES

OPEN ACCESS

RECEIVED
20 August 2025

REVISED
28 October 2025

ACCEPTED FOR PUBLICATION
30 November 2025

PUBLISHED
17 December 2025

PERSPECTIVE

Accelerated discovery of multinary chalcogenide quantum dots: combining aqueous chemistry with high-throughput experimentation and machine learning

Oleksandr Stroyuk[1,*], **Oleksandra Raievska**[1], **Dietrich R T Zahn**[2,3] and **Christoph J Brabec**[1,4]

[1] Forschungszentrum Jülich GmbH, Helmholtz-Institut Erlangen Nürnberg für Erneuerbare Energien (HI ERN), 91058 Erlangen, Germany
[2] Semiconductor Physics, Chemnitz University of Technology, 09107 Chemnitz, Germany
[3] Center for Materials, Architectures, and Integration of Nanomembranes (MAIN), Chemnitz University of Technology, 09107 Chemnitz, Germany
[4] Friedrich-Alexander-Universität Erlangen-Nürnberg, Materials for Electronics and Energy Technology (i-MEET), Martensstrasse 7, 91058 Erlangen, Germany
[*] Author to whom any correspondence should be addressed.

E-mail: o.stroyuk@fz-juelich.de

Keywords: quantum dots, sustainable synthesis, high-throughput experimentation, autonomous material screening, self-driving lab, metal-chalcogenide semiconductors

Abstract

Multinary chalcogenide quantum dots (MCQDs) exhibit unprecedented variability in composition and properties, size tunability, and high tolerance to multiple alloying, doping, and deviations from stoichiometry. This variability enables the synthesis of hundreds of thousands of MCQDs, characterized by a wide range of composition- and size-dependent spectral and photophysical properties, with a high potential for optoelectronic applications. At that, the whole compositional richness of MCQDs can be readily accessed using sustainable aqueous chemistry. The present Perspective focuses on the challenges of navigating the vast compositional space of MCQDs to discover new optoelectronic materials for the absorption, emission, and conversion of light. We argue that the exploration of the compositional versatility of MCQDs requires accelerated research, going beyond the conventional intuition-driven experiments. The acceleration can be achieved by high-throughput parallelized experimentation that yields extensive datasets and enables machine-learning-driven data analysis and automation of the targeted discovery of new MCQDs.

1. Introduction

The physics and chemistry of semiconductor quantum dots (QDs) are fascinating and promising research areas showing successful development for almost 40 years, crowned in 2023 by the Nobel Prize in chemistry awarded to M. Bawendi, L. Brus, and A. Ekimov [1–3]. The laureates initiated a broad exploration of the quantum size effects for tuning the optoelectronic properties of nanocrystalline (NC) semiconductors without actual modifications of their chemical composition, at the same time showing a high potential of 'wet' chemistry for the synthesis of inorganic semiconductor QDs [1–7].

Originally discovered for halide semiconductor NCs, the quantum size effects were soon reported for binary covalent II–VI and IV–VI compounds, such as cadmium and lead chalcogenides [2–4, 8, 9]. Later, more complex compositions were added to the 'focus group' of QDs, in particular multinary (ternary, quaternary) chalcopyrites and kesterites, such as $CuInS_2$ (CIS), $AgInS_2$ (AIS), and Cu_2ZnSnS_4 (CZTS) [9–16]. The exploration of multinary chalcogenide QDs (MCQDs) revealed many unique properties of these materials, with no close analogs in the physico-chemistry of binary QDs [9, 11, 14–17]. In particular, MCQDs demonstrated an unprecedented compositional variability stemming from a high tolerance to off-stoichiometry and formation of solid solutions, as well as to lattice disordering, defects, and

dopants [17, 18]. At that, typical MCQDs show remarkable size dependences of the optoelectronic, photophysical, and (photo)chemical properties in the size range of 1–10 nm, which is readily accessible by 'wet' chemical approaches [8, 9, 11, 14, 15, 19–24].

The studies of composition- and size-selected MCQDs quickly evolved from purely academic interest to practical applications related to the generation, conversion, and storage of light energy, with a clear focus on solution-processed and printable devices [21, 25, 26]. The most prominent examples include light-emissive materials for bio-sensing, LEDs, and light management [11–13, 16, 17, 19, 24, 27, 28], photo(electro)catalytic systems [9, 11, 14–16, 29, 30], and QD-based solar cells [10, 11, 16, 18, 20, 21, 25, 30–34].

The implementation of MCQDs in the opto-electronic devices revealed a large space of parameters available for optimization for every single MCQD composition, for example, the disordering of QD lattice, type and thickness of protecting wider-bandgap shells, and type and density of surface ligands [9, 10, 12–14, 17, 18, 22–24, 31]. Efficient navigation and exploration of this parameter space requires a significant acceleration of the material screening [35–38]. In the present Perspective, we argue that the accelerated exploration of MCQDs can be achieved by a combination of automated robot-assisted experimentation, data-driven prediction, and decision-making executed by artificial intelligence (AI) [35–37, 39]. We provide an overview of the unique compositional variability of the MCQDs, focusing on the potential and scope of aqueous chemistry-based approaches available for the efficient exploration of this versatile material domain. Using selected examples of the high-throughput screenings of MCQDs performed in our lab, we highlight the aqueous chemistry of MCQDs as a powerful platform for future AI-driven autonomous exploration workflows.

2. Compositional versatility of MCQDs

Multinary AMX_2 QDs reveal extraordinary compositional variability, originating from their high tolerance to multiple alloying and non-stoichiometry, and allowing for broad variations at each of the available sites, A, M, and X [9, 11–15, 17, 22, 23, 27, 28]. Even for the stoichiometric AMX_2 compositions, tens of different QDs can be synthesized by introducing Ag^+, Cu^+, Na^+, etc to the A site, In^{3+}, Bi^{3+}, Sb^{3+}, or Fe^{3+} to the M site, and choosing X among S, Se, or Te (figure 1). For any of these compounds, independent alloyings are possible by combining two or more cations in the A and M positions, as well as by mixing different chalcogenide anions in the X position. These alloyings result essentially in new compounds, which share the same lattice type but feature unique spectral and photophysical properties, increasing the number of possible MCQDs to ca. 10^3 (figure 1).

As the MCQDs allow large deviations from the AMX_2 stoichiometry, any of the MCQDs can be produced as a series of non-stoichiometric A_x–M_y–$X_{(x+3y)/2}$ (or simply A–M–X) QDs with broadly varied A:M ratios, increasing the population of MCQDs to ca. 10^4. Both AMX_2 and A–M–X QDs can be further modified by a shell of wider-bandgap semiconductor materials [8, 11, 19], the shell materials including Y = ZnS, MnS, GaS_x, etc, elevating the compositional variability of core/shell (A–M–X)@Y QDs by an order of magnitude (figure 1).

Finally, every core A–M–X and core/shell (A–M–X)@Y QD ensemble can be subjected to post-synthesis size selection, yielding a series of QDs with the same composition, but different size/size distribution and exhibiting different spectral and photophysical properties due to quantum size effects [11, 13, 14, 22, 23, 27, 32]. Considering that typical size-selection procedures allow about ten different fractions of MCQDs to be separated, the total number of individual nano-objects again increases to ca. 10^6 (figure 1).

One of the aims of this Perspective is to show that this enormous compositional space can be harnessed by mild approaches of aqueous chemistry, combining the sustainability of synthetic procedures with a reliable control over the structure, composition, size, and surface chemistry of MCQDs [8, 14, 17, 19, 22, 23]. Figure 1 provides examples of luminescent colloidal MCQDs produced in aqueous solutions, including a family of $AInS_2$ QDs with A = Cu, Ag, or Hg, alloyed core/shell $Cu_xAg_{1-x}InS_2$@ZnS (ZCAIS) QDs with a varied Cu/Ag ratio, a family of (Ag–In–S)@ZnS (ZAIS) QDs with varied Ag:In ratio, a series of core/shell (Cu–In–S)@ZnS (ZCIS) QDs with a varied ZnS shell thickness, as well as two examples of size-selected ZAIS QD series.

3. Harnessing the compositional versatility of MCQDs by aqueous chemistry

This section aims to illustrate the rich array of different tools available within the aqueous chemistry of MCQDs for varying and controlling their composition and electronic properties. These tools include

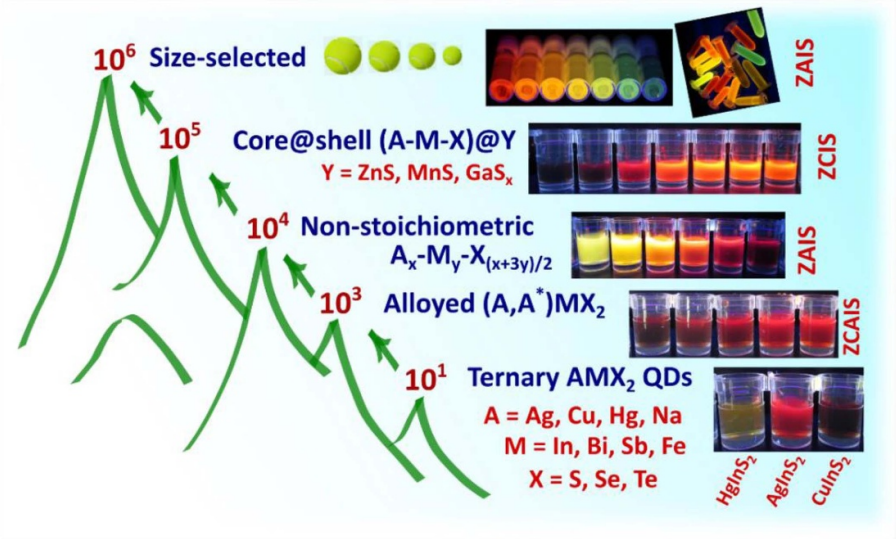

Figure 1. Gradual increase in complexity of MCQDs through various magnifying factors, including alloying, off-stoichiometry, shelling, and size selection. Photographs provide examples of colloidal MCQDs produced in our group by aqueous chemistry (photographs were collected under UV illumination).

(i) tuning MCQD properties by synthetic variables and (ii) modifying the MCQDs by post-synthesis treatments.

3.1. Variable parameters of the aqueous synthesis of MCQDs

The protocols of the aqueous synthesis of colloidal MCQDs are relatively flexible and allow a wide range of parameters to be varied. This range includes, but is not limited to: (i) independent compositional variation of A, M, and X sites in AMX_2 QDs; (ii) variations of component ratios in non-stoichiometric A–M–X QDs; (iii) alloying of several components on each of the A, M, or X positions; (iv) variations of ligands and shell materials and thickness.

Compositional variations in stoichiometric MCQDs can be performed at all three positions—A, M, and X, as illustrated by figures 2(a)–(c). A typical example is the A variation in AMX_2 (figure 2(a)), yielding isostructural chalcopyrites $AgInS_2$ (AIS), $CuInS_2$ (CIS), and $HgInS_2$ (HIS), as well as corresponding core/shell QDs [40–44]. Isovalent variations on the M position are more challenging for aqueous protocols in view of the low hydrolytic stability of Ga^{3+}, Bi^{3+}, or Fe^{3+} precursors. At the same time, a formal substitution of $2In^{3+}$ with $Zn^{2+}+Sn^{4+}$ transforms chalcopyrite CIS QDs to kesterite Cu_2ZnSnS_4 (CZTS) QDs (figure 2(b)) [44–48]. The iso-ligand CIS and CZTS QDs produced by an aqueous synthesis show a very similar structural motif (figure 2(b), insert) and similar size distributions [44, 47, 49, 50].

The substitutions on the X site can be exemplified by $AgInS_xSe_{1-x}$ (AISSe) QDs with freely variable x (figure 2(c)) [51]. At that, the sustainable character of the aqueous synthesis is maintained by *in situ* generating Se^{2-} via the disproportionation of Na_2SeSO_3 [51].

Off-stoichiometry is a unique feature of the MCQDs, distinguishing them from II–VI or IV–VI QDs, such as CdSe or PbS [14, 17]. Due to a high tolerance to defects and vacancies, the ratios of A and M can be extensively varied, yielding isostructural chalcopyrite QDs with different electronic and spectral properties [14, 15, 17, 23]. The strongest impact is typically exerted by varying the A/M ratio [40–43, 47, 50, 52–57], as illustrated by figure 2(d) for CIS, AIS, and ZAIS QDs, where the Cu(Ag):In ratio can be tuned from 1:10 (or even 1:20) to 1:1, producing MCQDs with bright PL ranging from green to brown, red, and deep red colors (figure 2(d)).

Alloying of two or more metals on A or M sites of AMX_2 and A–M–X QDs allows the electronic and spectral properties of MCQDs to be varied [14, 17, 22, 23], as exemplified by (Cu_xAg_{1-x})–In–S (CAIS) QDs (figure 2(e)). The solid-solution CAIS QDs reveal linear evolution of the lattice parameters with x (insert in figure 2(e)) [44, 58, 59], but narrower band gaps of mixed CAIS and ZCAIS QDs as compared to those of Cu- or Ag-only QDs, with the lowest E_g values observed at around Cu:Ag = 1:1 (figure 2(e)). This band-bowing behavior is general for Cu/Ag-mixed MCQDs and typically accounted for by local lattice disordering and inhomogeneities [58].

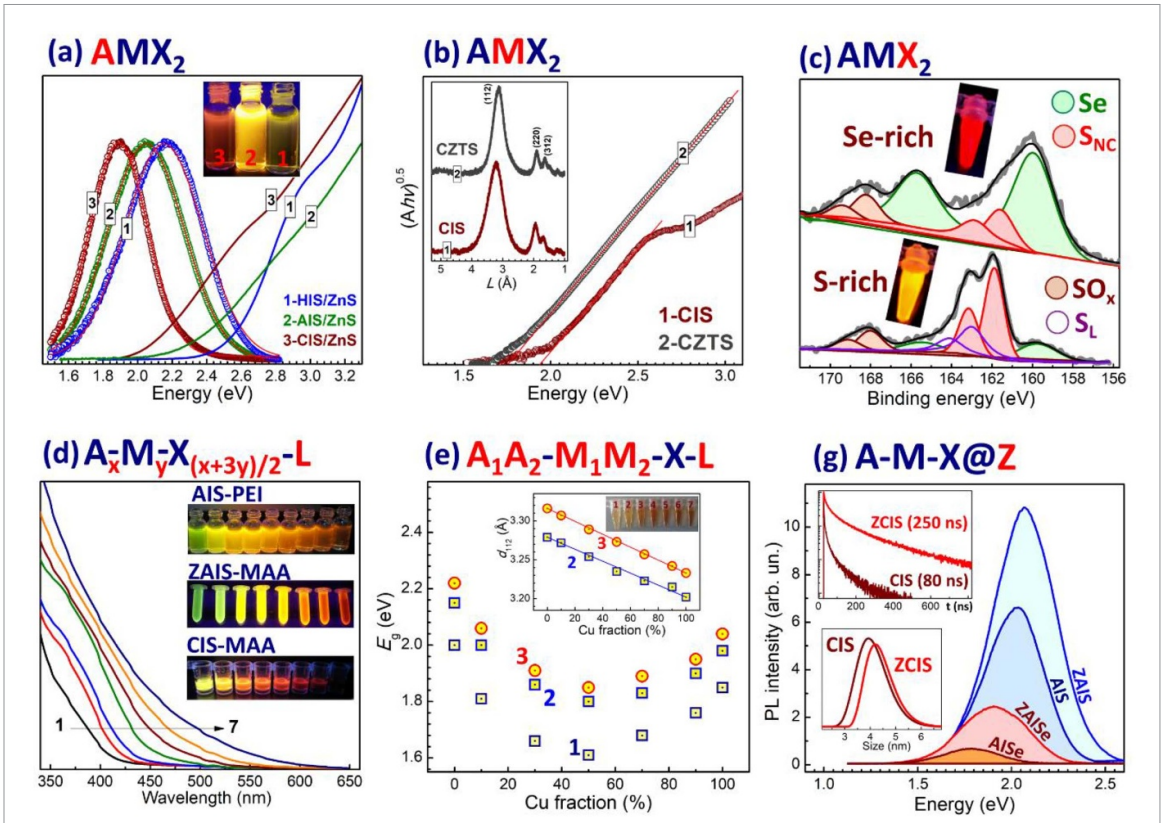

Figure 2. Overview of variable parameters during the synthesis of MCQDs. (a) Absorption (solid lines 1–3) and PL spectra (scatters 1–3) of AMX_2/ZnS QDs with A = Hg (1), Ag (2), and Cu (3); insert shows photographs of the HIS (1), AIS (2), and CIS (3) colloids under UV illumination. (b) Absorption spectra in Tauc coordinates for indirect transitions (main figure) and XRD profiles (insert) of CIS QDs (1) and CZTS QDs (2). (c) X-ray photoelectron spectra for colloidal sulfur-rich and selenium-rich $AgIn(S,Se)_2$ QDs. Inserts show photographs of corresponding colloidal solutions under UV illumination (350–390 nm). (d) Absorption spectra of PEI-stabilized AIS QDs with Ag/In ratio of 0.1 (curve 1), 0.2 (2), 0.3 (3), 0.5 (4), 0.7 (5), 0.9 (6), and 1.0 (7). The insert shows exemplary photographs of AIS-PEI, ZAIS-MAA, and CIS-MAA QDs with A:In ratio increasing from left (0.1) to right (1.0) under UV excitation. (e) Bandgap (main figure) and (112) interplanar distance (insert) of CAIS-MAA QDs (scatter 1), CAIS-GSH QDs (2), and ZCAIS-GSH QDs (3) as functions of the nominal Cu content. Solid lines in the insert correspond to linear fits, and the photographs show a series of ZCAIS QDs under ambient illumination. (g) PL spectra of AISe, ZAISe, AIS, and ZAIS QDs. Inserts show PL decay curves (upper panel) and hydrodynamic size (lower panel) of CIS and ZCIS QDs.

The examples presented in figures 2(d) and (e) illustrate a variability of surface ligands in aqueous syntheses of MCQDs. Similar approaches can be adapted either for the synthesis of positively charged MCQDs capped by polyethylene imine (PEI) [14, 44, 52] or negatively charged MCQDs capped by mercaptoacetate anions (MAA) [40, 41, 44, 53, 55, 59] or glutathione (GSH) [44, 55, 56] as shown in figure 2(d). The stability of metal complexes with anionic ligands determines the size and size distribution of the final MCQDs, resulting in different bandgaps of MAA- and GSH-capped ZCAIS QDs of the same composition (figure 2(e), scatters 1,2).

The deposition of a wider-bandgap shell on MCQDs, typically ZnS, results in the strong enhancement of the radiative recombination in MCQDs due to the passivation of surface defects by the shell and volume defects by diffusing Zn^{2+} [14, 15, 22, 23]. The PL enhancement factors vary from tens to hundreds of percent depending on defect population in the core MCQDs (figure 2(g), upper insert). The deposition of a ZnS shell is typically achieved by introducing Zn^{2+} complexes with the same sulfur-containing ligand (MAA, GSH, etc), which decompose under a mild thermal treatment, forming sub-nanometer ZnS shells (figure 2(g), lower insert) [40, 41, 44, 53–55, 59]. The shell formation is accompanied by a partial alloying of ZnS into the core QDs, increasing the bandgap of the core/shell QDs as compared to the core counterparts (figure 2(g)).

3.2. Post-synthesis variables

Size-selective precipitation/redispersion. Aqueous syntheses of colloidal MCQDs typically produce ensembles of QDs with sizes distributed between ca. 1 and 5–6 nm [14, 40, 56], which have different surface area, surface ligand density, and stability to precipitation. These variations allow the ensemble to be resolved into fractions with different average QD sizes by gradually lowering the general solubility of the QDs via step-wise additions of antisolvents, such as aliphatic alcohols. Upon the addition of

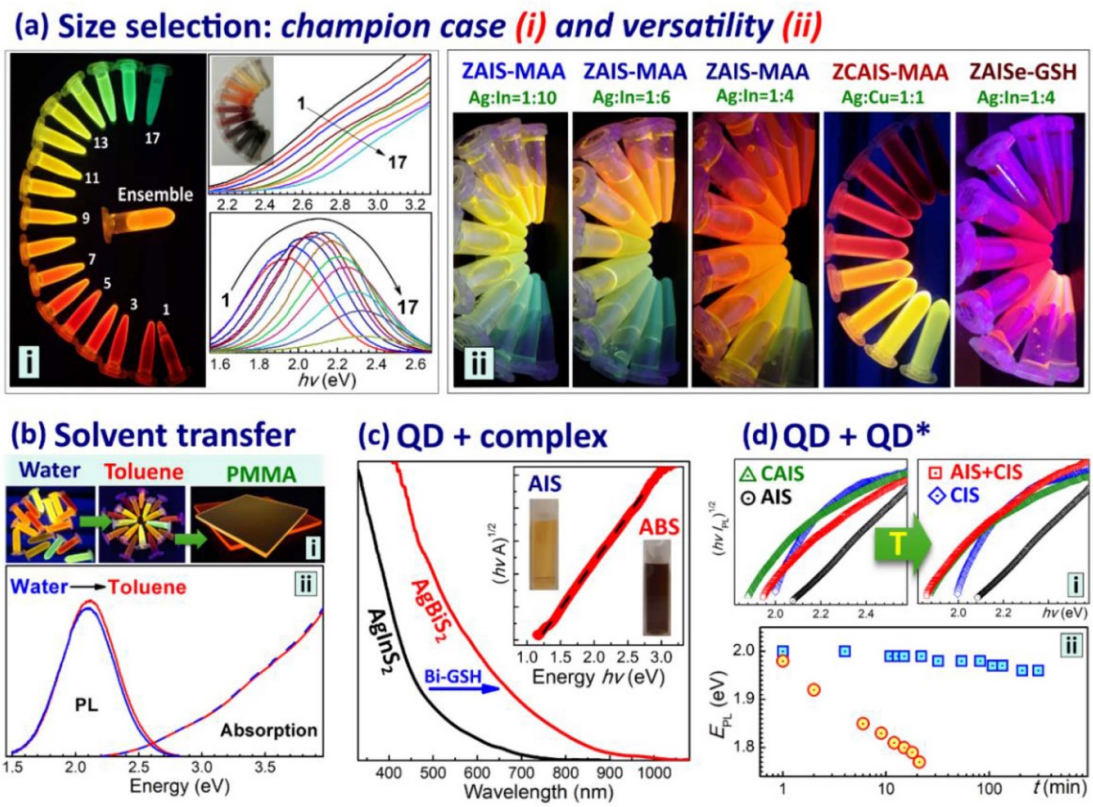

Figure 3. Overview of post-synthesis treatments of MCQDs. (a) Examples of size selection of colloidal MCQDs: (i) the 'champion' case of 17 size-selected fractions produced from a single MCQD ensemble (photograph under UV illumination, absorption spectra, and PL spectra); (ii) a set of cases showing general applicability of the size selection for ZAIS-MAA QDs with different Ag:In ratios of 1:10, 1:6, and 1:4, for ZCAIS-MAA QDs, and ZAISe-GSH QDs. (b) Solvent transfer of ZAIS-GSH QDs from water to toluene to the PMMA matrix: photographs under UV illumination (i), and normalized absorption/PL spectra (ii). (c, d) Examples of post-synthesis alloying of (c) AIS-GSH QDs with a Bi^{3+}-GSH complex and (d) colloidal AIS-GSH and CIS-GSH QDs in their mixture. In (d): (i) absorption spectra of CIS, AIS, CAIS QDs, and a mixture of CIS + QIS QDs before (left panel) and after the thermal treatment at 98 °C (right panel); (ii) evolution of the PL band maximum E_{PL} of a mixture of CIS + AIS QDs at room temperature (squares) and 98 °C (circles).

small antisolvent portions, the largest MCQDs in the ensemble precipitate, and by repeating this stepwise addition of the antisolvent and collecting the precipitates, a series of size-selected QD fractions with decreasing average size and narrower size distributions can be isolated. As the 1–6 nm MCQDs show medium-to-strong spatial exciton confinement, the size selection procedure yields collections of QD fractions with strongly different spectral properties, but the same composition [14, 40, 41, 44, 47, 51, 56, 57, 60, 61]. Figure 3(a-i) shows a 'champion' case of size-selection of ZAIS QDs, where up to 17 fractions of QDs were separated with PL emission colors ranging from deep red to green and bluish green for the smallest QDs. The antisolvent-driven size selection is a universal approach and can be applied to MCQDs with various compositions, stoichiometries, and size distributions. By combining size-selection with a compositional design, for example, with variations of the Ag:In ratio in the non-stoichiometric ZAIS QDs, Cu:Ag in the alloyed ZCAIS QDs, or the S:Se ratio in ZAISSe QDs, highly emissive MCQDs with a very broad gamut of PL colors can be produced, as exemplified by figure 3(a-ii).

Solvent transfer. The MCQDs precipitated by antisolvents can be redispersed in hexane or toluene, in the presence of additional ligands, such as oleylamine and oleic acid, with no changes in the PL QYs (figure 3(b-i)) or spectral characteristics (figure 3(b-ii)). This transferability allows the luminescent MCQDs to be incorporated into polymer matrices for light-management applications (figure 3(b-i)) [61, 62].

Increasing the MCQD complexity by post-synthesis alloying. Aqueous MCQDs capped by molecular ligands form an equilibrium with metal-ligand complexes, for example, with Ag(I)-GSH and In(III)-GSH complexes in the case of AIS-GSH QDs. Such equilibria enable size-selection procedures and result in many unique properties of aqueous MCQDs, such as a high sensitivity to ambient temperature [14, 22, 23, 40, 44, 55] or spontaneous cation exchanges with other metal complexes. As an example, $AgInS_2$-GSH QDs can be transformed into $AgBiS_2$-GSH QDs by introducing an excess of Bi^{3+}-GSH complex (figure 3(c)).

When two sorts of MCQDs with the same ligand are brought into contact, the equilibria between the QDs and metal-ligand complexes interact, resulting in a new state of equilibrium and gradual alloying of the two QD types into a more complex compound. In this way, GSH-capped CIS and AIS QDs spontaneously alloy into CAIS QDs [63, 64]. This process can be tracked spectrally due to the band-bowing behavior of mixed CAIS QDs (figure 3(d-i)). The alloying starts already at ambient conditions, accelerating considerably at higher temperatures (figure 3(d-ii)) [63, 64].

4. Accelerated discovery of MCQDs—automated and autonomous experimentation

The compositional versatility of MCQDs, accessible through mild aqueous chemistry, reveals a large potential for exploring hundreds of thousands of NC materials. This variability is further elevated by going from materials to devices, due to a large number of variable parameters to be tuned for the optimal performance of MCQDs in various optoelectronic applications. The exploration of the experimental spaces of such dimensions requires innovative approaches, going far beyond the conventional 'trial and error' research, by making the speed of exploration commensurate with the number of variables.

Recent efforts in this direction show several promising approaches to the acceleration of the material screening, including (i) high-throughput (HTP) robot-assisted experimentation, (ii) automated/autonomous experimentation guided by AI, and (iii) high-performance *ab initio* calculations capable of precise targeting of the most promising materials. Here we will focus on the first two experimental approaches, referring the readers to the recent reviews [65–70] on the computational material screening.

The HTP experimentation can be realized by delegating most of the synthetic procedures to robots, capable of performing hundreds of combinatorial syntheses and post-synthesis treatments of MCQDs in parallel by general protocols. The combinatorial HTP synthesis is typically complemented by HTP characterization, for example, by inline spectroscopies. Two examples of the HTP workflows based on aqueous syntheses of MCQDs are presented below in section 4.1. Further acceleration of the HTP materials screening can be achieved by applying AI tools, in particular, machine learning (ML) for the analysis of the experimental data and identification of the most promising directions for the next experiments. Ultimately, the ML tools can be used to explore beyond the tested compositional domain by data-driven predictions and to suggest new experimental parameters/conditions to achieve the target QD properties with a minimal number of experiments. A combination of ML-driven experiment planning with fully automated robot-driven synthesis and characterization is expected to result in loop-like workflows, capable of autonomous material screening with minimal human intervention, as discussed in section 4.2.

4.1. HTP screening of MCQDs

As shown in section 3.1, the variations of synthesis parameters of MCQDs and post-synthesis treatments can be performed within the same general synthetic protocol under open-environment conditions [14, 22], allowing these procedures to be realized using a pipetting robot instructed to screen through all possible combinations of multiple precursors. In this section, two examples of HTP combinatorial screening of MCQDs are discussed, focusing on (i) a family of core AIS and core/shell ZAIS QDs with varied size and Ag:In ratio (figure 4(a)) and (ii) a library of $Cu_xAg_{1-x}InS_ySe_{1-y}$@ZnS (ZCAISSe) QDs produced by spontaneous alloying of AIS, CIS, AISe, and CISe QD precursors (figure 4(b)). The HTP screening of aqueous MCQDs was performed with a four-nozzle pipetting robot with a three-dimensional freedom of movement, programmed to collect and dispense precursors, dilute QD solutions for spectral measurements, transfer core QDs into a separate station for shell deposition and film formation, and assist in size-selective precipitation [64]. A typical robot configuration shown in figure 4(b-ii) includes a pre-configured precursor station (1), a shaking station (2), a heating station (3), auxiliary stations for post-synthesis manipulations (4), a robotic nozzle set (5), and a plate-reading spectrometer for inline acquisition of absorption, PL, and PL excitation (PLE) spectra.

In the first HTP screening campaign (figure 4(a)), this platform was applied to produce arrays of AIS and ZAIS QDs with Ag:In ratio and average size varied along the *Y* and *X* axes of the array, respectively (figure 4(a-i)). The sample arrays, both as original solutions, films, and colloidal solutions regenerated from solid films, were subjected to spectral HTP characterization, including absorption, PL/PLE, and time-resolved PL measurements with automated plate-reading setups [60]. In this way, ca. 200 samples can be produced and tested within 2 d, allowing the photophysical characteristics of AIS and ZAIS QDs to be mapped versus the QD bandgap [60]. As an outcome, the optimal bandgap range, ca. 2.1–2.2 eV, was found with maximal PL QYs of up to ca. 55% (figure 4(a-ii)), as well as linear relationships between the QD bandgap and the average lifetimes (figure 4(a-iii)).

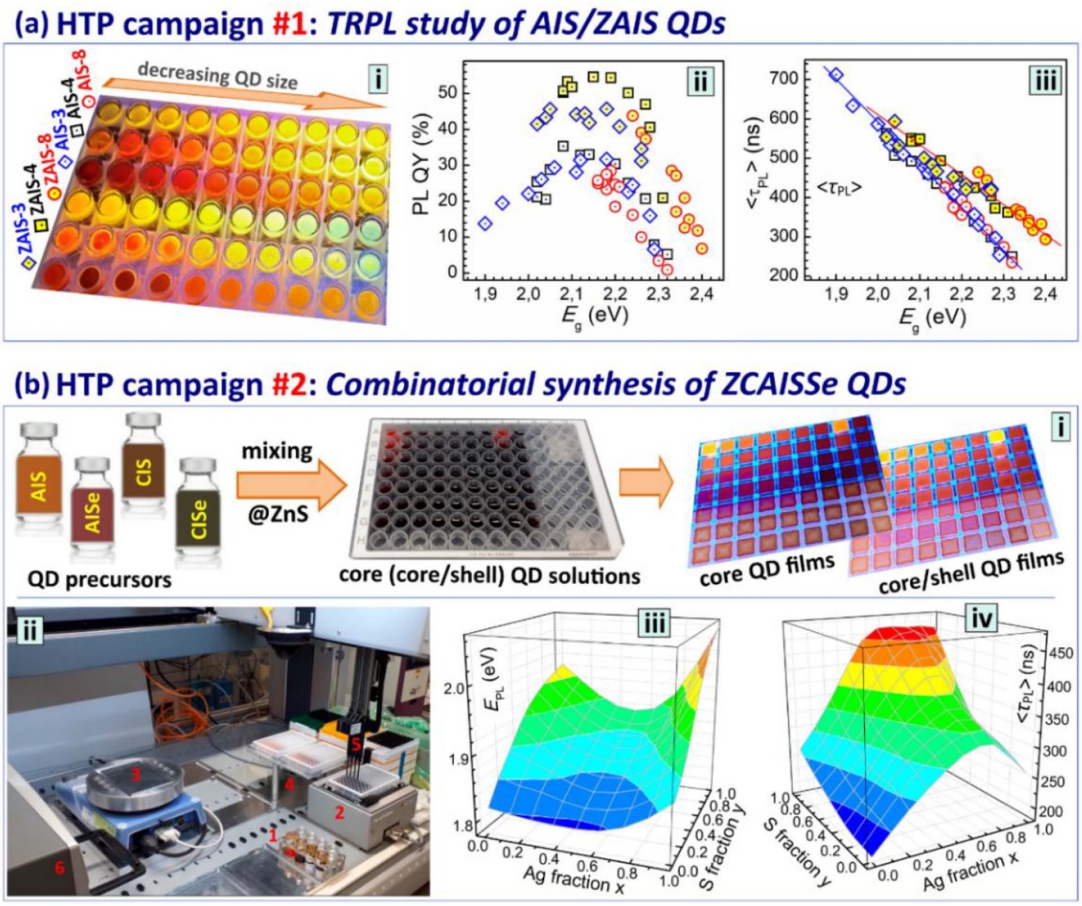

Figure 4. Overview of the HTP screenings of size- and composition-selected aqueous MCQDs. (a) HTP study of spectral and photophysical properties of AIS/ZAIS QDs: (i) photograph of the array of dried samples under UV illumination; (ii, iii) PL QY (ii) and average PL lifetime $\langle\tau_{PL}\rangle$(iii) as functions of the QD bandgap. (b) Robot-assisted HTP screening of $Cu_xAg_{1-x}InS_ySe_{1-y}$ (CAISSe) and core@ZnS QDs: (i) scheme of the HTP workflow; (ii) photograph of a robotic setup used for the HTP synthesis of ZCAISSe QDs; (iii, iv) compositional maps of E_{PL} (iii) and $\langle\tau_{PL}\rangle$(iv).

In the second HTP campaign (figure 4(b)), four types of precursor QDs, AIS, AISe, CIS, and CISe, with the same ligand (GSH or MAA), were subjected to a combinatorial robot-assisted alloying in all possible binary, ternary, and quaternary combinations. Then, CAISSe QDs were alloyed with a Zn^{2+}-ligand complex, resulting in corresponding core/shell ZCAISSe QDs and collected as colloidal solutions and drop-cast films (figure 4(i)) [64]. Analysis of absorption and PL data in the library revealed a general band-bowing behavior both for CAISSe and ZCAISSe QDs (figure 4(b-iii)) [58, 64]. The average PL lifetime also showed non-additive dependences on the QD composition, demonstrating maximal values at Ag:Cu = approximately 1:1 and increasing with the molar fraction of sulfur (figure 4(b-iv)) [64].

4.2. Accelerated discovery of MCQDs by autonomous lab workflows

The HTP workflows can produce at least two orders of magnitude larger data arrays, as compared to human-driven experiments, resulting in ever-increasing scale of data analysis. This challenge can be met by applying different AI-based instruments, in particular, ML and large language models, to mine big experimental data arrays in search of hidden relationships between input synthesis parameters and properties of final materials [35–38, 71]. The ML tools are well-suited for chemical applications, while ML can directly process experimental data in various forms (tables, graphs, images, etc) in situations when physical relationships between the experimental variables and outcomes are unknown [71]. Typically, ML algorithms are applied to (i) predict new datapoints starting from an existing dataset and (ii) to plan new experiments based on previously collected datapoints.

Prediction aims to establish a mathematical relationship between the properties of materials (for example, size and bandgap of QDs) and a set of experimental conditions (for example, type and ratio of precursors, temperature, etc) [71]. The ML-driven prediction allows a large dataset to be generated from a much smaller experimental dataset [72, 73] or literature reports [74, 75]. For example, gradient boosting and random forest models were found to efficiently predict dependences between the PL band

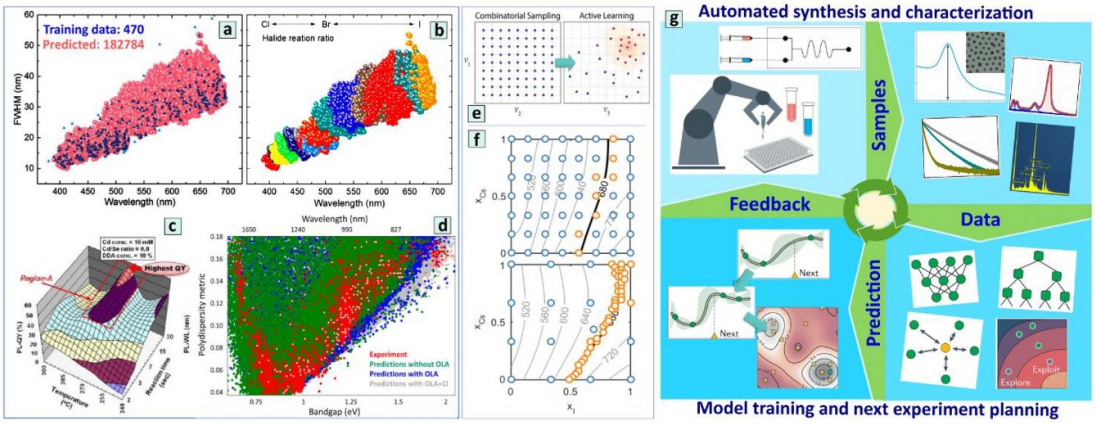

Figure 5. (a)–(d) Examples of ML-driven prediction of the synthesis outcome of lead-halide perovskite NCs (a), (b), CdSe QDs (c), and PbS QDs (d). (e) A scheme of sampling in combinatorial and active-learning-driven NC synthesis. (f) Comparison between systematic screening (upper graph) and active-learning-guided sample selection (lower graph) in the microfluidic synthesis of perovskite NCs. (a), (b) [72] John Wiley & Sons. © 2022 The Authors. Advanced Photonics Research published by Wiley-VCH GmbH. (c) Reprinted with permission from [77]. Copyright (2012) American Chemical Society. (d) Reprinted with permission from [78]. Copyright (2019) American Chemical Society. (e) Reproduced from [37] with permission from the Royal Society of Chemistry. (f) Reprinted with permission from [79]. Copyright (2018) American Chemical Society. (g) Reproduced from [71], with permission from Springer Nature.

maximum wavelength and spectral width of lead-halide perovskite NCs, allowing the experimental dataset of 470 datapoints to be expanded into a predicted dataset of more than 180 000 datapoints generated within the experimentally probed range (figure 5(a)) [72]. This larger dataset can then be used to visualize 'rules of the synthesis', that is, dependences between experimental parameters and PL properties (figure 5(b)) [72]. An ML model was trained on ca. 300 experiments with Cs–Pb–Br perovskite QDs and was able to predict ca. 500 000 datapoints for a detailed mapping of composition and phase as functions of precursors feed ratio [76].

An artificial neural network (ANN) trained on the synthesis of 256 batches of CdSe QDs was able to predict ca. 5000 new datapoints for mechanistic studies of the QD formation [73]. A similar ANN-based approach was applied to a dataset of 1500 datapoints collected in the combinatorial synthesis of CdSe QDs with six variables, generating a set of ca. 26 000 predicted datapoints for 'parameter-property' mapping [77], identifying a domain of reaction conditions, yielding the highest PL QYs (figure 5(c)).

The ML algorithms allow the accumulated data to be used more efficiently, providing a 'data pool' for the AI-assisted extraction of hidden 'synthesis parameter—QD property' relationships. As an example, an ML model was trained using 2300 experimental datapoints collected during 6 years of PbS QD syntheses, revealing the most significant factors that define the ratio of QD nucleation and growth rates (figure 5(d)) [78].

Experiment-planning ML algorithms focus on efficient data collection and workflow optimization, suggesting next experiments and optimal synthesis conditions for the required outcome [35–38, 71]. The most popular experiment-planning ML algorithm, Bayesian optimization, was specifically developed for cost- and time-intensive experiments, reaching targets with the minimal number of trials. The ability of ML to suggest new experimental conditions allows the experimentation and modeling to be orchestrated in a loop, where every new experiment is used to retrain the model and derive the next synthetic step—the concept typically referred to as 'active learning' (AL). The training starts from a sparse and random initial variable grid, yielding a predictive map of the target parameters (figure 5(e)), showing the most promising parameters of the next experiment. The suggestion is experimentally verified, and the model is retrained, eventually resulting in the new suggestion, with the entire process performed iteratively until the target property of QDs is reached.

The number of iterations depends on the system complexity, number of variables, and the size of the starting dataset, typically remaining below 30–50 cycles, thus providing a considerable acceleration in the material discovery as compared to the combinatorial HTP screening. For example, the AL-guided autonomous microfluidic screening of lead-halide NCs started from a sparse grid of 16 datapoints (figure 5(f), upper panel), identified ca. 40 parameter combinations leading to a target property in 10–12 iterations, while the conventional systematic gridding revealed only 8 target compositions (figure 5(f), lower panel) [79]. A similar AL-based microfluidic workflow was developed for the synthesis of lead-halide NCs, handling ten variables with ca. 10^7 potential parameter combinations and identifying

optimal conditions for the synthesis of 10 compositions with targeted PL maxima within one hour of operation [80].

The concept of an autonomous or self-driving lab has rapidly developed over the last years, being considered as one of the most significant technological developments, revolutionizing the field of material discovery [36–38, 67, 81–84]. With the acceleration of material discovery as one of the main aims, the self-driving labs are often referred to as material acceleration platforms (MAPs), deployed for screenings of organic semiconductors [85, 86], metal-halide perovskites [85–87], and metal-chalcogenide QDs [36, 88]. The MAP concept integrates automated synthesis and characterization with AL-driven decision-making and experiment planning into closed-loop operation (figure 5(g)) [38, 39, 67, 84, 85, 89]. The automated synthesis generates materials, subjected to automated characterization to train a model for the prediction of new conditions and the next cycle of experiments, until the target property is achieved [67, 83].

Automated synthesis is typically organized along two different concepts: (i) microfluidic synthesis and (ii) robot-assisted human-mimicking synthesis. The microfluidic synthesis is perfectly suited for liquid NC materials [90], including metal-chalcogenide QDs [36, 91–94], metal NCs [91], and metal-halide perovskite NCs [72, 76, 79, 80, 92, 95–98]. It combines rapid and homogeneous mass and heat transfer, inline detection tools, and a large potential for upscaling [90, 91, 93, 99].

The concept of a human-mimicking automated synthesis is realized in two versions: (a) as a robotized platform integrating manipulators, pipettes, vial-handlers, heaters, shakers, and inline characterizations [38, 81, 82, 100], and (b) as a modular system including conventional laboratory workplaces united by a human-mimicking robot that transfers samples between the stations [38, 81, 84, 101]. The human-mimicking platforms provide high flexibility in the state of samples, being adaptable for the formation of thin films [89, 100, 102] and solid-state reactions [101]. The integrated robotic systems were successfully applied for the automated synthesis of chalcogenide QDs [73, 78, 88, 103, 104], metal NCs [105, 106], while their potential for the automated synthesis of MCQDs is still to be explored and evaluated.

Automated characterization includes inline methods, such as absorption, PL, or Raman spectroscopies [81, 82, 84, 97] with the human-mimicking robots providing access to a wider spectrum of off-line tools, for example, x-ray diffraction, mass spectrometry, x-ray photoelectron spectroscopy, energy-dispersive x-ray spectroscopy, nuclear magnetic resonance, etc [38, 81, 89, 100]. The human-mimicking systems can also be coupled with HTP modules for the characterization of the functional properties, such as photo(electro)chemical [107–109] or electrochemical activity [110, 111], as well as with automated lines for the production and testing of functional devices, for example, solar cells [112–114].

5. Summary and outlook

MCQDs reveal an extraordinary variability of composition, high tolerance to substitutions and doping, lattice disordering, and deviations from the AMX_2 stoichiometry. This compositional flexibility offers versatile ways to tune the opto-electronic properties by independently varying QD composition and QD size, resulting in a myriad of possible combinations with different electronic, spectral, and photophysical properties. In contrast to the mature state of the research of II–VI and IV–VI semiconductor QDs, the exploration of the vast compositional space of MCQDs is still at the uprising stages, mostly focusing on a few selected combinations, such as CIS(Se), AIS(Se), and CZTS, already revealing a high potential of these MCQDs for energy conversion. In this view, further exploration of MCQDs is expected to be a high-gain research venue for novel MCQD-based materials for existing and new applications, especially those related to light conversion and emission. The navigation of the vast compositional space of MCQDs and discovery of novel materials can be considerably accelerated by upscaling the 'trial and error' strategy to a new HTP level, both by massive parallelization of the synthesis/characterization, and by automation and ML-guided experiment planning.

The HTP experimentation combines the excellent performance of modern robotic materials screening platforms with the capacities of compositional design of MCQDs provided by mild aqueous chemistry, which is perfectly compatible with the commercially available robots. The HTP synthesis/characterization of MCQDs is a powerful instrument for accelerated build-up of massive datasets on the 'composition-property' rules of MCQDs, which can then be used by AI-based tools for predictions of new MCQD-based materials and orchestrating autonomous experimentation. The autonomous materials screening workflows realized by self-driving labs or MAPs will bring material discovery to a qualitatively new level of efficiency and depth. The MAPs offer (i) unrivaled experimental precision and reproducibility, (ii) accelerated feedback on the functionality of new materials in different applications by combining MAPs

with device acceleration platforms (DAPs), and (iii) seamless integration of the experimentation and computations into hybrid workflows, where further material discovery acceleration can be achieved by creating and exploiting virtual digital twins of real experimental processes. The potential of MAPs was demonstrated for a few classes of nanomaterials, including inorganic semiconductor and halide perovskite NCs. While the applicability of MAPs to explore metal-chalcogenide QDs was proven for II–VI and IV–VI chalcogenide QDs, the broad and systematic autonomous screening of MCQDs remains a mission for future studies.

In this view, the present Perspective is an appeal of the authors to raise broader interest and awareness of the great potential of the accelerated research of MCQDs. Simultaneously, it outlines the state-of-the-art in this field, serving as a starting point and a background for the practical realization of the concept of the autonomous discovery of new MCQD-based materials. In this concept, we aim to integrate our previous experience in the accelerated solution-processed screening of organic, hybrid, and inorganic semiconductors, machine-learning-based prediction and experiment-planning algorithms, and PV-oriented DAPs, allowing for automated optimization of solar cells into a fully autonomous lab to discover new MCQD-based materials for energy conversion applications. This lab will be capable of efficient exploration of the compositional space of MCQDs, providing a large dataset on the MCQD properties, and simultaneously pushing us up along the learning curve by continuous evolution of the automated experimentation and the decision-making AI algorithms. The exploitation of such an automated lab will shape a medium-to-long-term strategy for further development of the field.

Some promising components of this strategy can already be outlined at the present stage of development. For example, the complexity of MCQDs is expected to reach the domain of *high-entropy compounds*, combining 7–8 elements in comparable molar ratios and featuring new properties, untypical of the less complex materials [115–121]. A 'cocktail' effect of random mixing of multiple components results in high stability of high-entropy compounds, flexibility and disordering of the lattice, and a variety of active sites available for catalytic, electrocatalytic, and photo(electro)catalytic reactions [117, 118, 121]. The effects of crystal size and spatial exciton confinement on the functional properties, naturally expected for high-entropy MCQDs, are still to be characterized and interpreted.

The spatial confinement in QDs results in clearly defined sets of quantized energy levels, featuring MCQDs as 'artificial atoms' with a unique composition/size-dependent electronic configuration [2–4, 11]. The autonomous discovery of MCQDs is expected to yield a large library of artificial MCQD 'atoms', available for building *self-assembled superlattices* with advanced optoelectronic and charge transport properties [122, 123]. Going from discrete QDs to QD superlattices will bring the MCQD-based material design to a new level of complexity and variability by self-assembly of different sorts of artificial atoms.

The strategy of autonomous research can go beyond MCQDs and include *combinations of different material classes*, in particular, chalcogenide and halide semiconductor QDs, into a new family of chalcohalides as a natural successor of MCQDs and metal-halide perovskite NCs [124–126]. In parallel, the conventional role of organic surface ligands can be expanded by introducing *new ligands with multiple functionalities*, including charge and energy exchanges with the QD core, modulating dark and photoinduced redox-activity of MCQDs, facilitating charge transport in the QD superlattices, providing QDs with chemical selectivity or bio-compatibility, etc [127]. This approach is brilliantly exemplified by light upconversion through triplet-triplet annihilation in rationally designed 'QD-molecule' assemblies [127–129].

In summary, the autonomous materials discovery of MCQD-based materials shows highly promising future perspectives going far beyond the immediate compositional screening of individual MCQDs and providing ample 'anchoring points' to other chemistries and material classes.

Data availability statement

No new data were created or analysed in this study.

Author contributions

Oleksandr Stroyuk 0000-0001-5054-2746
Conceptualization (lead), Writing – original draft (lead)

Oleksandra Raievska
Investigation (lead), Methodology (equal), Writing – review & editing (equal)

Dietrich R T Zahn 0000-0002-8455-4582
Conceptualization (equal), Funding acquisition (equal), Project administration (equal), Resources (equal), Writing – review & editing (equal)

Christoph J Brabec
Conceptualization (equal), Funding acquisition (equal), Project administration (equal), Resources (equal), Writing – review & editing (equal)

References

[1] Sarma D D and Kamat P V 2023 2023 Nobel Prize in chemistry: a mega recognition for nanosized quantum dots *ACS Energy Lett.* **8** 5149–51
[2] Manna L 2023 The bright and enlightening science of quantum dots *Nano Lett.* **23** 9673–6
[3] Efros A L and Brus L E 2021 Nanocrystal quantum dots: from discovery to modern development *ACS Nano* **15** 6192–210
[4] Brus L 1986 Electronic wave functions in semiconductor clusters: experiment and theory *J. Phys. Chem.* **90** 2555–60
[5] Kortan A R, Hull R, Opila R L, Bawendi M G, Steigerwald M L, Carroll P J and Brus L E 1990 Nucleation and growth of CdSe on ZnS quantum crystallite seeds, and vice versa, in inverse micelle media *J. Am. Chem. Soc.* **112** 1327–32
[6] Murray C B, Norris D J and Bawendi M G 1993 Synthesis and characterization of nearly monodisperse CdE (E = sulfur, selenium, tellurium) semiconductor nanocrystallites *J. Am. Chem. Soc.* **115** 8706–15
[7] Rossetti R and Brus L 1982 Electron-hole recombination emission as a probe of surface chemistry in aqueous CdS colloids *J. Phys. Chem.* **86** 4470–2
[8] Jing L, Kershaw S V, Li Y, Huang X, Li Y, Rogach A L and Gao M 2016 Aqueous-based semiconductor nanocrystals *Chem. Rev.* **116** 10623–730
[9] Wu L, Li Y, Liu G-Q and Yu S-H 2024 Polytypic metal chalcogenide nanocrystals *Chem. Soc. Rev.* **53** 9832–73
[10] Wang J, Liu J, Yin H, Li S, Kuvondikov V and Ye L 2023 Eco-friendly and ultrathin solar cells featuring nanocrystals: advances and perspectives *Mater. Chem. Front.* **7** 4693–706
[11] Roy P, Mukherjee A, Mondal P, Bhattacharyya B, Narayan A and Pandey A 2022 Electronic structure and spectroscopy of I–III–VI2 nanocrystals: a perspective *J. Phys. Chem. C* **126** 7364–73
[12] Chen B, Pradhan N and Zhong H 2018 From large-scale synthesis to lighting device applications of ternary I–III–VI semiconductor nanocrystals: inspiring greener material emitters *J. Phys. Chem. Lett.* **9** 435–45
[13] Yang L, Zhang S, Xu B, Jiang J, Cai B, Lv X, Zou Y, Fan Z, Yang H and Zeng H 2023 I–III–VI quantum dots and derivatives: design, synthesis, and properties for light-emitting diodes *Nano Lett.* **23** 2443–53
[14] Stroyuk O *et al* 2018 Solar light harvesting with multinary metal chalcogenide nanocrystals *Chem. Soc. Rev.* **47** 5354–422
[15] Stroyuk O 2017 Solar light harvesting with nanocrystalline semiconductors *Lecture Notes in Chemistry Series* (Springer) p 378
[16] Jin L, Selopal G S, Tong X, Perepichka D F, Wang Z M and Rosei F 2024 Heavy-metal-free colloidal quantum dots: progress and opportunities in solar technologies *Adv. Mater.* **36** 2402912
[17] Wang L, Yin Z and Tang A 2024 Component engineering in multinary alloyed I-III-VI type semiconductor nanocrystals for photoluminescence and electroluminescence *Acc. Mater. Res.* **5** 1210–20
[18] Du Z and Ma D 2025 Recent progress in I-III-VI colloidal quantum dots-integrated solar cells *Curr. Opin. Colloid Interface Sci.* **75** 101890
[19] Islas-Rodriguez N, Muñoz R, Rodriguez J A, Vazquez-Garcia R A and Reyes M 2023 Integration of ternary I-III-VI quantum dots in light-emitting diodes *Front. Chem.* **11** 1106778
[20] Palchoudhury S, Ramasamy K and Gupta A 2020 Multinary copper-based chalcogenide nanocrystal systems from the perspective of device applications *Nanoscale Adv.* **2** 3069–82
[21] Azimi H, Hou Y and Brabec C J 2014 Towards low-cost, environmentally friendly printed chalcopyrite and kesterite solar cells *Energy Environ. Sci.* **7** 1829–49
[22] Stroyuk O *et al* 2020 Unique luminescent properties of composition-/ size-selected aqueous Ag-In-S and core/shell Ag-In-S/ZnS quantum dots *Core/Shell Quantum Dots. Lecture Notes in Nanoscale Science and Technology* ed X Tong and M Wang vol 28 (Springer)
[23] Stroyuk O, Raievska O, Zahn D R T and Brabec C J 2024 Exploring highly efficient broadband self-trapped-exciton luminophors: from 0D to 3D materials *Chem. Rec.* **24** e202300241
[24] Lu H, Carroll G M, Neale N R and Beard M C 2019 Infrared quantum dots: progress, challenges, and opportunities *ACS Nano* **13** 939–53
[25] Turnley J W and Agrawal R 2024 Solution processed metal chalcogenide semiconductors for inorganic thin film photovoltaics *Chem. Commun.* **60** 5245–69
[26] Fu M and Critchley K 2024 Inkjet printing of heavy-metal-free quantum dots-based devices : a review *Nanotechnology* **35** 302002
[27] Knowles K E, Hartstein K H, Kilburn T B, Marchioro A, Nelson H D, Whitham P J and Gamelin D R 2016 Luminescent colloidal semiconductor nanocrystals containing copper: synthesis, photophysics, and applications *Chem. Rev.* **116** 10820–51
[28] Zhou J, Yang Y and Zhang C 2015 Toward biocompatible semiconductor quantum dots: from biosynthesis and bioconjugation to biomedical application *Chem. Rev.* **115** 11669–717
[29] Wang K, Tao Y, Tang Z, Zhao H, Sun X, Rosei F, Liu D and Xiong Y 2025 Stability of photoelectrochemical cells based on colloidal quantum dots *Chem. Soc. Rev.* **54** 3513–34
[30] Santos D R, Shukla S and Vermang B 2023 Prospects of copper–bismuth chalcogenide absorbers for photovoltaics and photoelectrocatalysis *J. Mater. Chem. A* **11** 22087–104
[31] Akhil S and Balakrishna R G 2022 AgBiS2 as a photoabsorber for eco-friendly solar cells: a review *J. Mater. Chem. A* **10** 8615–25
[32] Yang B, Cang J, Li Z and Chen J 2024 Nanocrystals as performance-boosting materials for solar cells *Nanoscale Adv.* **6** 1331–60
[33] Rehman F, Syed I H, Khanam S, Ijaz S, Mehmood H, Zubair M, Massoud Y and Mehmood M Q 2023 Fourth-generation solar cells: a review *Energy Adv.* **2** 1239–62
[34] Lin S and Peng X 2021 Current status and challenges of solar cells based on semiconductor nanocrystals *Energy Fuels* **35** 18928–41
[35] Lv H and Chen X 2022 Intelligent control of nanoparticle synthesis through machine learning *Nanoscale* **14** 6688–708

[36] Munyebvu N, Lane E, Grisan E and Howes P D 2022 Accelerating colloidal quantum dot innovation with algorithms and automation *Mater. Adv.* **3** 6950–67

[37] Szymanski N J, Zeng Y, Huo H, Bartel C J, Kim H and Ceder G 2021 Toward autonomous design and synthesis of novel inorganic materials *Mater. Horiz.* **8** 2169–98

[38] Bayley O, Savino E, Slattery A and Noël T 2024 Autonomous chemistry: navigating self-driving labs in chemical and material sciences *Matter* **7** 2382–98

[39] Xie Y, Sattari K, Zhang C and Lin J 2023 Toward autonomous laboratories: convergence of artificial intelligence and experimental automation *Prog. Mater. Sci.* **132** 101043

[40] Raievska O, Lesnyak V, Haubold D, Dzhagan V, Stroyuk O, Gaponik N, Zahn D R T and Eychmüller A 2017 A fine size selection of brightly luminescent water-soluble Ag-In-S and Ag-In-S/ZnS quantum dots *J. Phys. Chem. C* **121** 9032–42

[41] Raievska O, Rosovik O, Kozytskiy A, Stroyuk O, Dzhagan V and Zahn D R T 2016 Non-stoichiometric Cu-In-S@ZnS nanoparticles produced in aqueous solutions as light harvesters for liquid-junction photoelectrochemical solar cells *RSC Adv.* **6** 100145–57

[42] Stroyuk O, Raevskaya A, Spranger F, Selyshchev O, Dzhagan V, Solonenko D, Gaponik N, Zahn D R T and Eychmüller A 2019 Mercury-indium-sulfide nanocrystals: a new member of the family of ternary in-based chalcogenides *J. Chem. Phys.* **151** 144701

[43] Dzhagan V, Selyshchev O, Raievska O, Stroyuk O, Hertling L, Mazur N, Valakh M Y and Zahn D R T 2020 Phonon spectra of strongly luminescent nonstoichiometric Ag–In–S, Cu–In–S, and Hg–In–S nanocrystals of small size *J. Phys. Chem. C* **124** 15511–22

[44] Raievska A, Stroyuk O and Kuchmiy S 2017 Nanoparticles of Ag–In–S and Cu–In–S in aqueous media: preparation, spectral and luminescent properties *Theor. Exp. Chem.* **53** 338–48

[45] Selyshchev O, Havryliuk Y, Valakh M Y, Yukhymchuk V O, Raievska O, Stroyuk O L, Dzhagan V and Zahn D R T 2020 Raman and x-ray photoemission identification of colloidal metal sulfides as potential secondary phases in nanocrystalline Cu_2ZnSnS_4 photovoltaic absorbers *ACS Appl. Nano Mater.* **3** 5706–17

[46] Havryliuk Y, Selyshchev O, Valakh M, Raevskaya A, Stroyuk O, Schmidt C, Dzhagan V and Zahn D R T 2019 Raman study of flash-lamp annealed aqueous Cu_2ZnSnS_4 nanocrystals *Beilstein. J. Nanotechnol.* **10** 222–7

[47] Stroyuk O, Raevskaya A, Selyshchev O, Dzhagan V, Gaponik N, Zahn D R T and Eychmüller A 2018 "Green" aqueous synthesis and advanced spectral characterization of size-selected Cu_2ZnSnS_4 nanocrystal inks *Sci. Rep.* **8** 13677

[48] Havryliuk Y, Valakh M Y, Dzhagan V, Greshchuk O, Yukhymchuk V, Raevskaya A, Stroyuk O, Selyshchev O, Gaponik N and Zahn D R T 2018 Raman characterization of Cu_2ZnSnS_4 nanocrystals: phonon confinement effect and formation of CuxS phases *RSC Adv.* **8** 30736–46

[49] Dzhagan V, Selyshchev O, Kondratenko S, Mazur N, Havryliuk Y, Raievska O, Stroyuk O and Zahn D R T 2022 Copper-content dependent structural and electrical properties of CZTS films formed by "green" colloidal nanocrystals *Electron. Mater.* **3** 136–53

[50] Vorona I *et al* 2021 Room-temperature electron paramagnetic resonance study of copper-related defect in Cu2ZnSnS4 colloidal nanocrystals *J. Phys. Chem. C* **125** 9923–9

[51] Raievska O, Stroyuk O, Dzhagan V, Solonenko D and Zahn D R T 2020 Ultra-small aqueous glutathione-capped Ag–In–Se quantum dots: luminescence and vibrational properties *RSC Adv.* **10** 42178–93

[52] Raievska O, Ivanchenko M V, Skoryk M A and Stroyuk O L 2016 Brightly luminescent colloidal Ag-In-S nanoparticles stabilized in aqueous solutions by branched polyethyleneimine *J. Lumin.* **178** 295–300

[53] Raievska O, Ivanchenko M, Stroyuk O, Kuchmiy S Y and Plyusnin V F 2015 Luminescent Ag-doped In_2S_3 nanoparticles stabilized by mercaptoacetate in water and glycerol *J. Nanopart. Res.* **17** 135

[54] Stroyuk O, Dzhagan V, Raievska O, Spranger F, Gaponik N and Zahn D R T 2019 Insights into different photoluminescence mechanisms of binary and ternary aqueous nanocrystals from the temperature dependence: a case study of CdSe and Ag-In-S *J. Lumin.* **215** 116630

[55] Stroyuk O, Raevskaya A, Spranger F, Gaponik N and Zahn D R T 2019 Temperature-dependent photoluminescence of silver-indium-sulfide nanocrystals in aqueous colloidal solutions *ChemPhysChem* **20** 1640–8

[56] Stroyuk O, Raevskaya A, Spranger F, Selyshchev O, Dzhagan V, Schulze S, Zahn D R T and Eychmüller A 2018 Origin and dynamics of highly efficient broadband photoluminescence of aqueous glutathione-capped size-selected Ag−In−S quantum dots *J. Phys. Chem. C* **122** 13648–58

[57] Raievska O, Rozovik O P, Kozytskiy A V, Stroyuk O L and Gaponik N 2017 Photo-electrochemical characteristics of nanoheterostructures based on titanium dioxide and Ag-In-S quantum dots produced by size-selective precipitation *Theor. Exp. Chem.* **53** 251–8

[58] Raievska O, Stroyuk O, Azhniuk Y, Solonenko D, Barabash A, Brabec C J and Zahn D R T 2020 Composition-dependent optical band bowing, vibrational, and photochemical behavior of aqueous glutathione-capped (Cu, Ag)–In–S quantum dots *J. Phys. Chem. C* **124** 19375–88

[59] Raievska O, Rozovik O, Novikova A, Selyshchev O, Stroyuk O, Dzhagan V, Goryacheva I, Gaponik N, Zahn D R T and Eychmüller A 2018 Luminescence and photoelectrochemical properties of size-selected aqueous copper-doped Ag–In–S quantum dots *RSC Adv.* **8** 7550–7

[60] Stroyuk O, Raievska O, Kupfer C, Solonenko D, Osvet A, Batentschuk M, Brabec C J and Zahn D R T 2021 High-throughput time-resolved photoluminescence study of composition- and size-selected aqueous Ag–In–S quantum dots *J. Phys. Chem. C* **125** 12185–97

[61] Stroyuk O, Weigert F, Raievska O, Spranger F, Würth C, Resch-Genger U, Gaponik N and Zahn D R T 2019 Inherently broadband photoluminescence in Ag−In−S/ZnS quantum dots observed in ensemble and single-particle studies *J. Phys. Chem. C* **123** 2632–41

[62] Dhamo L, Carulli F, Nickl P, Wegner K D, Hodoroaba V, Würth C, Brovelli S and Resch-Genger U 2021 Efficient luminescent solar concentrators based on environmentally friendly Cd-free ternary AIS/ZnS quantum dots *Adv. Opt. Mater.* **9** 2100587

[63] Stroyuk O, Raievska O, Solonenko D, Kupfer C, Osvet A, Batentschuk M, Brabec C J and Zahn D R T 2021 Spontaneous alloying of ultrasmall non-stoichiometric Ag–In–S and Cu–In–S quantum dots in aqueous colloidal solutions *RSC Adv.* **11** 21145–52

[64] Stroyuk O *et al* 2021 High-throughput robotic synthesis and photoluminescence characterization of aqueous multinary copper-silver indium chalcogenide quantum dots *Part. Part. Syst. Charact.* **38** 21001689

[65] Curtarolo S, Hart G L W, Nardelli M B, Mingo N, Sanvito S and Levy O 2013 The high-throughput highway to computational materials design *Nat. Mater.* **12** 191–201

[66] Cole J M 2020 A design-to-device pipeline for data-driven materials discovery *Acc. Chem. Res.* **53** 599–610

[67] Pyzer-Knapp E O, Pitera J W, Staar P W J, Takeda S, Laino T, Sanders D P, Sexton J, Smith J R and Curioni A 2022 Accelerating materials discovery using artificial intelligence, high performance computing and robotics *npj Comput. Mater.* **8** 84

[68] Chen C *et al* 2024 Accelerating computational materials discovery with machine learning and cloud high-performance computing: from large-scale screening to experimental validation *J. Am. Chem. Soc.* **146** 20009–18

[69] Oganov A R, Pickard C J, Zhu Q and Needs R J 2019 Structure prediction drives materials discovery *Nat. Rev. Mater.* **4** 331–48

[70] Pyzer-Knapp E O, Manica M, Staar P, Morin L, Ruch P, Laino T, Smith J R and Curioni A 2025 Foundation models for materials discovery—current state and future directions *npj Comput. Mater.* **11** 61

[71] Tao H, Wu T, Aldeghi M, Wu T C, Aspuru-Guzik A and Kumacheva E 2021 Nanoparticle synthesis assisted by machine learning *Nat. Rev. Mater.* **6** 701–16

[72] Chen G *et al* 2023 Machine learning-assisted microfluidic synthesis of perovskite quantum dots *Adv. Photon. Res.* **4** 2200230

[73] Xu R H J, Keating L P, Vikram A, Shim M and Kenis P J A 2024 Understanding hot injection quantum dot synthesis outcomes using automated high-throughput experiment platforms and machine learning *Chem. Mater.* **36** 1513–25

[74] Li J, Chen T, Lim K, Chen L, Khan S A, Xie J and Wang X 2019 Deep learning accelerated gold nanocluster synthesis *Adv. Intell. Syst.* **1** 1900029

[75] Nguyen H A *et al* 2022 Predicting indium phosphide quantum dot properties from synthetic procedures using machine learning *Chem. Mater.* **34** 6296–311

[76] Chairil R, Forsberg A P, Brutchey R L and Malmstadt N 2025 High-throughput reaction discovery for Cs–Pb–Br nanocrystal synthesis *React. Chem. Eng.* **10** 398–406

[77] Orimoto Y, Watanabe K, Yamashita K, Uehara M, Nakamura H, Furuya T and Maeda H 2012 Application of artificial neural networks to rapid data analysis in combinatorial nanoparticle syntheses *J. Phys. Chem. C* **116** 17885–96

[78] Voznyy O, Levina L, Fan J Z, Askerka M, Jain A, Choi M-J, Ouellette O, Todorović P, Sagar L K and Sargent E H 2019 Machine learning accelerates discovery of optimal colloidal quantum dot synthesis *ACS Nano* **13** 11122–8

[79] Bezinge L, Maceiczyk R M, Lignos I, Kovalenko M V and Demello A J 2018 Pick a color MARIA: adaptive sampling enables the rapid identification of complex perovskite nanocrystal compositions with defined emission characteristics *ACS Appl. Mater. Interfaces* **10** 18869–78

[80] Abdel-Latif K, Epps R W, Bateni F, Han S, Reyes K G and Abolhasani M 2021 Self-driven multistep quantum dot synthesis enabled by autonomous robotic experimentation in flow *Adv. Intell. Syst.* **3** 2000245

[81] Tom G *et al* 2024 Self-driving laboratories for chemistry and materials science *Chem. Rev.* **124** 9633–732

[82] Abolhasani M and Kumacheva E 2023 The rise of self-driving labs in chemical and materials sciences *Nat. Synth.* **2** 483–92

[83] Qiu J, Zhu L, Feng Z, Luo Z and Wang L 2025 A revolutionary paradigm in chemistry and materials science research: self-driving laboratories *Chem. Commun.* **61** 10026–38

[84] Bennett J A and Abolhasani M 2022 Autonomous chemical science and engineering enabled by self-driving laboratories *Curr. Opin. Chem. Eng.* **36** 100831

[85] Zhang J, Wu J, Stroyuk O, Raievska O, Lüer L, Hauch J A and Brabec C J 2024 Self-driving AMADAP laboratory: accelerating the discovery and optimization of emerging perovskite photovoltaics *Mater. Res. Bull.* **49** 1284–94

[86] Zhang J, Hauch J A and Brabec C J 2024 Toward self-driven autonomous material and device acceleration platforms (AMADAP) for emerging photovoltaics technologies *Acc. Chem. Res.* **57** 1434–45

[87] Li J, Li J, Liu R, Tu Y, Li Y, Cheng J, He T and Zhu X 2020 Autonomous discovery of optically active chiral inorganic perovskite nanocrystals through an intelligent cloud lab *Nat. Commun.* **11** 2046

[88] Politi M, Baum F, Vaddi K, Antonio E, Vasquez J, Bishop B P, Peek N, Holmberg V C and Pozzo L D 2023 A high-throughput workflow for the synthesis of CdSe nanocrystals using a sonochemical materials acceleration platform *Digit. Discov.* **2** 1042–57

[89] Shahzad K *et al* 2024 Accelerating materials discovery: combinatorial synthesis, high-throughput characterization, and computational advances *Sci. Technol. Adv. Mater. Methods* **4** 2292486

[90] Saeed M M, Carthy E, Dunne N and Kinahan D 2025 Advances in nanoparticle synthesis assisted by microfluidics *Lab Chip* **25** 3060–93

[91] Sui J, Yan J, Liu D, Wang K and Luo G 2020 Continuous synthesis of nanocrystals via flow chemistry technology *Small* **16** 1902828

[92] Campbell Z S, Bateni F, Volk A A, Abdel-Latif K and Abolhasani M 2020 Microfluidic synthesis of semiconductor materials: toward accelerated materials development in flow *Part. Part. Syst. Charact.* **37** 2000256

[93] Jung J-Y, Lee J-G, Baek Y-K, Kim Y-D, Hong J-P and Kim Y-K 2019 High throughput process for the continuous preparation of quantum dots using fluid dynamically controlled reactor *J. Alloys Compd.* **784** 816–21

[94] Watanabe K, Orimoto Y, Nagano K, Yamashita K, Uehara M, Nakamura H, Furuya T and Maeda H 2012 Microreactor combinatorial system for nanoparticle synthesis with multiple parameters *Chem. Eng. Sci.* **75** 292–7

[95] Abdel-Latif K, Bateni F, Crouse S and Abolhasani M 2020 Flow synthesis of metal halide perovskite quantum dots: from rapid parameter space mapping to AI-guided modular manufacturing *Matter* **3** 1053–86

[96] Bateni F *et al* 2024 Smart dope: a self-driving fluidic lab for accelerated development of doped perovskite quantum dots *Adv. Energy Mater.* **14** 2302303

[97] Epps R W, Bowen M S, Volk A A, Abdel-Latif K, Han S, Reyes K G, Amassian A and Abolhasani M 2020 Artificial chemist: an autonomous quantum dot synthesis bot *Adv. Mater.* **32** 2001626

[98] Sadeghi S *et al* 2024 Autonomous nanomanufacturing of lead-free metal halide perovskite nanocrystals using a self-driving fluidic lab *Nanoscale* **16** 580–91

[99] Volk A A, Epps R W and Abolhasani M 2021 Accelerated development of colloidal nanomaterials enabled by modular microfluidic reactors: toward autonomous robotic experimentation *Adv. Mater.* **33** 2004495

[100] Ludwig A 2019 Discovery of new materials using combinatorial synthesis and high-throughput characterization of thin-film materials libraries combined with computational methods *npj Comput. Mater.* **5** 70

[101] Lunt A M *et al* 2024 Modular, multi-robot integration of laboratories: an autonomous workflow for solid-state chemistry *Chem. Sci.* **15** 2456–63

[102] Moradi S, Kundu S and Saidaminov M I 2022 High-throughput synthesis of thin films for the discovery of energy materials: a perspective *ACS Mater. Au.* **2** 516–24

[103] Salaheldin A M, Walter J, Herre P, Levchuk I, Jabbari Y, Kolle J M, Brabec C J, Peukert W and Segets D 2017 Automated synthesis of quantum dot nanocrystals by hot injection: mixing induced self-focusing *Chem. Eng. J.* **320** 232–43

[104] Chan E M, Xu C, Mao A W, Han G, Owen J S, Cohen B E and Milliron D J 2010 Reproducible, high-throughput synthesis of colloidal nanocrystals for optimization in multidimensional parameter space *Nano Lett.* **10** 1874–85

[105] Vaddi K, Chiang H T and Pozzo L D 2022 Autonomous retrosynthesis of gold nanoparticles via spectral shape matching *Digit. Discov.* **1** 502–10
[106] Yoo H J *et al* 2024 Bespoke metal nanoparticle synthesis at room temperature and discovery of chemical knowledge on nanoparticle growth via autonomous experimentations *Adv. Funct. Mater.* **34** 2312561
[107] Nursam N M, Wang X and Caruso R A 2015 High-throughput synthesis and screening of titania-based photocatalysts *ACS Comb. Sci.* **17** 548–69
[108] Kormányos A, Jenewein K J and Cherevko S 2022 High-throughput workflows in the service of (photo)electrocatalysis research *Trends Chem.* **4** 475–8
[109] Jenewein K J, Thienhaus S, Kormányos A, Ludwig A and Cherevko S 2022 High-throughput exploration of activity and stability for identifying photoelectrochemical water splitting materials *Chem. Sci.* **13** 13774–81
[110] Gerroll B H R, Kulesa K M, Ault C A and Baker L A 2023 Legion: an instrument for high-throughput electrochemistry *ACS Meas. Sci. Au.* **3** 371–9
[111] Xu X, Valavanis D, Ciocci P, Confederat S, Marcuccio F, Lemineur J-F, Actis P, Kanoufi F and Unwin P R 2023 The new era of high-throughput nanoelectrochemistry *Anal. Chem.* **95** 319–56
[112] Langner S, Häse F, Perea J D, Stubhan T, Hauch J, Roch L M, Heumueller T, Aspuru-Guzik A and Brabec C J 2020 Beyond ternary OPV: high-throughput experimentation and self-driving laboratories optimize multicomponent systems *Adv. Mater.* **32** 1907801
[113] Chen S *et al* 2018 Exploring the stability of novel wide bandgap perovskites by a robot based high throughput approach *Adv. Energy Mater.* **8** 1701543
[114] Gu E *et al* 2020 Robot-based high-throughput screening of antisolvents for lead halide perovskites *Joule* **4** 1806–22
[115] Huang E W, Lee W J, Singh S S, Kumar P, Lee C Y, Lam T N, Chin H H, Lin B H and Liaw P K 2022 Machine-learning and high-throughput studies for high-entropy materials *Mater. Sci. Eng. R* **147** 100645
[116] Zhou X, Mukoyoshi M and Kitagawa H 2025 Recent advances in high-entropy intermetallic nanoparticles: synthesis and electrocatalytic applications *Chem. Commun.* **61** 10911–30
[117] Liang Z, Yang Y, Tao Z, Gao R, Chen Y and Li P 2025 High-entropy materials for electrocatalytic oxygen reduction reaction *J. Mater. Chem. A* **13** 25195–212
[118] Shan B-F, Yang J, Xiang X and Zhao Z-Y 2025 High-entropy compounds for photo(electro)catalysis: diverse materials and applications *J. Mater. Chem. A* **13** 12808–27
[119] Zhao F, Zhang S and Sun X 2025 A perspective on the origin of high-entropy solid electrolytes *Adv. Mater.* **37** 1–9
[120] Schumacher S, Alekseev E V, Yu S, Tempel H and Eichel R 2025 High-entropy halides for intercalation battery electrode materials *ChemElectroChem* **12** 1–8
[121] Xie H, Yang Z, Liu J, Wu W, Huang T and Liu H 2025 High-entropy strategies for designing advanced solid-state electrolytes: a comprehensive review *Chem. Commun.* **61** 10449–69
[122] Boles M A, Engel M and Talapin D V 2016 Self-assembly of colloidal nanocrystals: from intricate structures to functional materials *Chem. Rev.* **116** 11220–89
[123] Liu M, Yazdani N, Yarema M, Jansen M, Wood V and Sargent E H 2021 Colloidal quantum dot electronics *Nat. Electron.* **4** 548–58
[124] Palazon F 2022 Metal chalcohalides: next generation photovoltaic materials? *Sol. RRL* **6** 2100829
[125] Ghorpade U V, Suryawanshi M P, Green M A, Wu T, Hao X and Ryan K M 2023 Emerging chalcohalide materials for energy applications *Chem. Rev.* **123** 327–78
[126] Zhang L, Meng X, Hu W, Liu F, Li D, Jia D, Ji Y, Li L and Qiu H 2025 Heteronanocrystals based on halide perovskites and chalcogenides *J. Phys. Chem. Lett.* **16** 7834–47
[127] Huang Z, Tung C H and Wu L Z 2024 Quantum dot-sensitized triplet-triplet annihilation photon upconversion for solar energy conversion and beyond *Acc. Mater. Res.* **5** 136–45
[128] Zeng L, Huang L, Han J and Han G 2022 Enhancing triplet-triplet annihilation upconversion: from molecular design to present applications *Acc. Chem. Res.* **55** 2604–15
[129] Niihori Y, Kosaka T and Negishi Y 2024 Triplet–triplet annihilation-based photon upconversion using nanoparticles and nanoclusters *Mater. Horiz.* **11** 2304–22